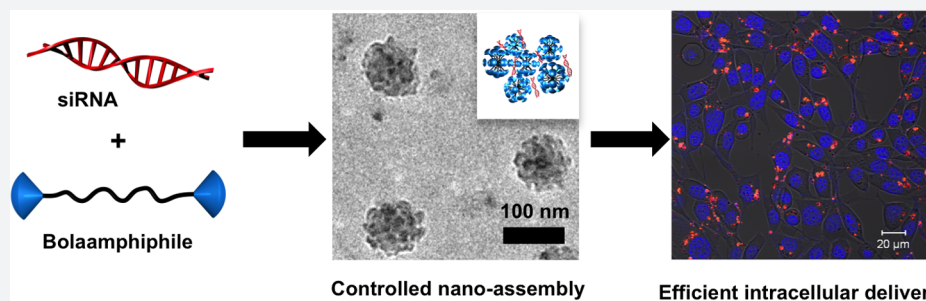


# Structure-Based Design of Dendritic Peptide Bolaamphiphiles for siRNA Delivery

Hanxiang Zeng<sup>†</sup>, Mark E. Johnson<sup>†</sup>, Nathan J. Oldenhuis, Timothy N. Tiambeng, and Zhibin Guan\*

Department of Chemistry, University of California, Irvine, California 92697, United States

 Supporting Information



**ABSTRACT:** Development of safe and effective delivery vectors is a critical challenge for the application of RNA interference (RNAi)-based biotechnologies. In this study we show the rational design of a series of novel dendritic peptide bolaamphiphile vectors that demonstrate high efficiency for the delivery of small interfering RNA (siRNA) while exhibiting low cytotoxicity and hemolytic activity. Systematic investigation into structure–property relationships revealed an important correlation between molecular design, self-assembled nanostructure, and biological activity. The unique bolaamphiphile architecture proved a key factor for improved complex stability and transfection efficiency. The optimal vector contains a fluorocarbon core and exhibited enhanced delivery efficiency to a variety of cell lines and improved serum resistance when compared to hydrocarbon analogues and lipofectamine RNAiMAX. In addition to introducing a promising new vector system for siRNA delivery, the structure–property relationships and “fluorocarbon effect” revealed herein offer critical insight for further development of novel materials for nucleic acid delivery and other biomaterial applications.

## INTRODUCTION

Since its discovery, RNA interference (RNAi) has demonstrated tremendous utility in a variety of biological applications, including experimental biology,<sup>1</sup> functional genomics,<sup>2</sup> stem cell research,<sup>3</sup> and treatment of diseases.<sup>4,5</sup> The high potency and specificity of gene silencing induced by small interfering RNA (siRNA) makes this technology particularly appealing for medicinal applications; however, safe and efficient delivery of siRNA into targeted cells remains a major challenge.<sup>5–7</sup> Much effort has been devoted to the development of synthetic delivery vectors<sup>8</sup> with a variety of systems being investigated, including lipids,<sup>9–11</sup> peptides,<sup>12–15</sup> polymers,<sup>16–19</sup> dendrimers,<sup>20,21</sup> and gold nanoparticles.<sup>22,23</sup> Cationic lipids (such as lipofectamine) and polymers (such as poly(ethylene imine), PEI) have been widely used in a variety of biological studies; however, toxicity and delivery efficiency are often limiting factors for these early vectors.<sup>24–26</sup> Recently lipid nanoparticles (LNPs)<sup>8,11,27</sup> and polymeric vectors<sup>16,28</sup> have demonstrated great promise for therapeutic delivery of siRNA to the liver and solid tumors. Despite major advances, the efficiency of endosomal escape of most vectors is generally low,<sup>29,30</sup> and interaction of conventional cationic lipids and polymers with the cell membrane can result in membrane disruption, altered cell behavior, and cytotoxicity.<sup>24,26,31–33</sup> While combinatorial approaches have proven useful for the discovery of new

vectors,<sup>10,34</sup> a deeper understanding of how structural parameters affect transfection efficiency, circulatory stability, serum resistance, and ultimately *in vivo* efficacy would be of great value for the further development of synthetic siRNA vectors. Toward this goal, a systematic approach based on direct structure–activity correlation should advance our basic understanding and facilitate the rational design of effective new vectors.

Herein we report the rational design of a dendritic peptide bolaamphiphile for safe and efficient siRNA delivery (Figure 1). Unlike regular lipid-like amphiphiles (termed “mono-amphiphile”), which are composed of one or more hydrophobic tails and a single hydrophilic headgroup, bolaamphiphiles (termed “bola”) are dumbbell-shaped molecules having two hydrophilic headgroups connected via a hydrophobic core (Figure 1a,b).<sup>35</sup> In nature, bolaamphiphiles are found in cell membranes of certain kinds of extremophile archaeabacteria with the monolayer assemblies, as opposed to the bilayer structures of normal lipids, providing improved stability under harsh conditions.<sup>36</sup> The robust self-assembly of bolaamphiphiles makes them attractive for biomaterials applications, with several recent reports of gene delivery using bolaamphiphile-based

Received: June 11, 2015

Published: August 14, 2015

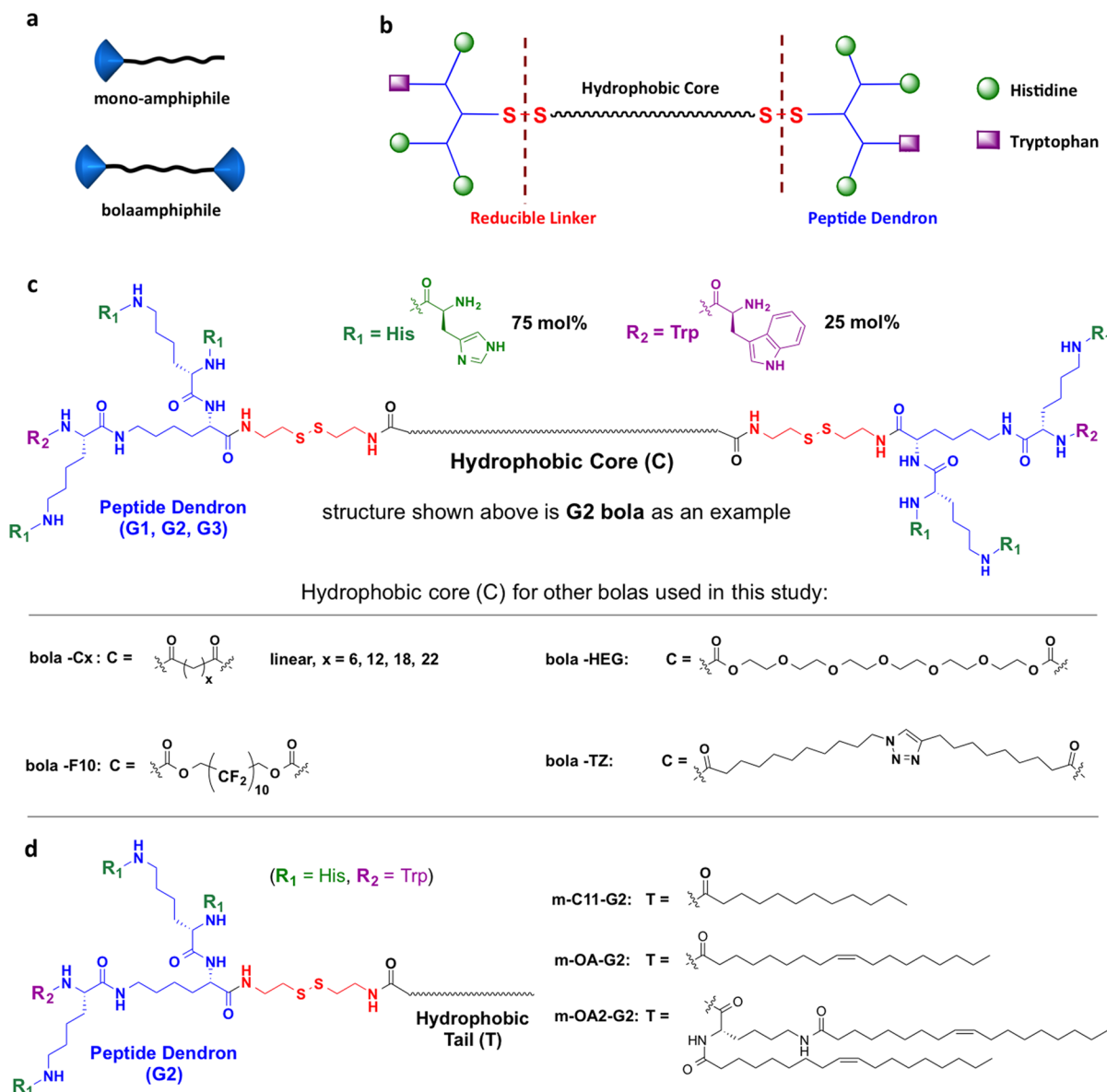


**Figure 1.** Design concept and structure of bolaamphiphiles. (a) Schematic illustration of mono-amphiphile and bolaamphiphile. (b) Design of dendritic peptide bolaamphiphiles. Bolaamphiphiles are composed of two dendritic peptide headgroups linked to a hydrophobic core by reducible disulfide linkages. The multifunctional dendritic peptide headgroups are functionalized with 75 mol % histidine (His) and 25 mol % tryptophan (Trp) on periphery. (c) Structures of dendritic peptide bolaamphiphiles. The structure of bola-C18-G2 is shown as an example. The dendritic peptide headgroups range from generation-1 (G1) to generation-3 (G3) dendrons. A series of hydrophobic cores as shown were used in the structure–property studies. (d) Structures of three dendritic peptide mono-amphiphiles used for comparative studies.

vectors.<sup>37–40</sup> We envision that the unique molecular architecture of bolas can be exploited to disfavor insertion into the cell membrane and offer a more biocompatible alternative to conventional lipids. The use of a hydrophobic core shorter than the native phospholipid bilayer should prevent direct membrane insertion due to unfavorable thermodynamics, with the use of relatively large dendritic headgroups to disfavor a U-shaped conformation (Figure 2a).

The second important design component is the choice of dendritic headgroup (Figure 1b,c), for which we chose a lysine-based dendron functionalized with 75 mol % histidine (His) and 25 mol % tryptophan (Trp), the optimal combination for our previous dendronized polymer vector.<sup>41</sup> The dendritic headgroup provides multivalent interactions for efficient binding of siRNA, with the size and valency controllable

through the use of different dendron generations. On the basis of our previous study, Trp improves siRNA binding and cell uptake, while His facilitates endosomal escape due to the pH-responsive nature of the imidazole ring.<sup>41</sup>

The third key component in our bola design is the hydrophobic core for promoting self-assembly in aqueous solution. As shown in Figure 1c, a variety of hydrophobic cores were studied by systematically changing several molecular parameters such as the length, geometry, and chemical nature. Given the unique self-assembly properties of fluorocarbons and previous reports on fluorinated vectors,<sup>42–46</sup> we envisioned that the fluorocarbon linker could promote robust self-assembly and also impact the cellular uptake, serum stability, and biodistribution of the complexes. The final design element is the disulfide linkages (Figure 1b,c), connecting the dendritic

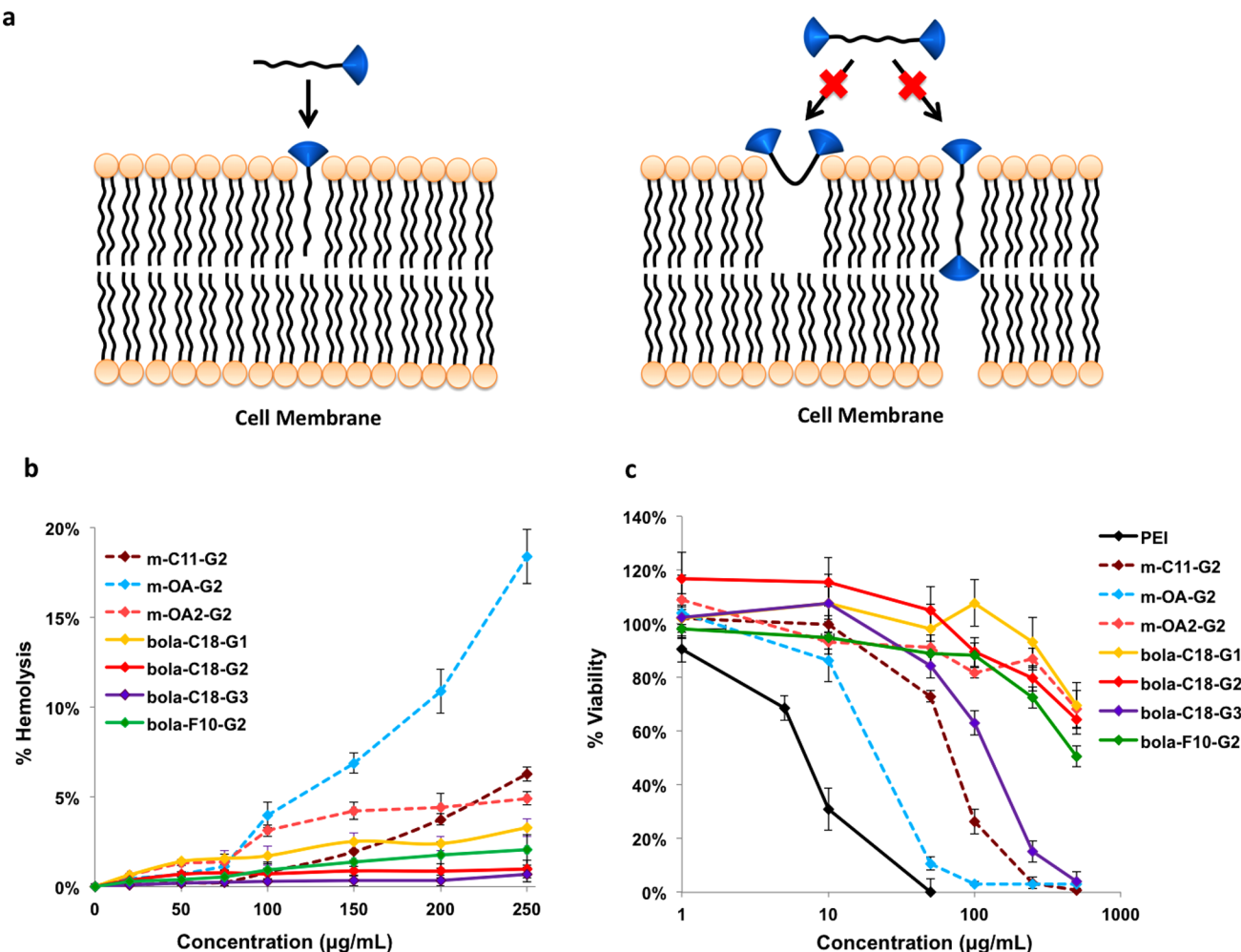


**Figure 2.** Hemolytic activity and cytotoxicity of bolaamphiphiles. (a) Proposed low membrane disruption character of dendritic bolaamphiphiles in comparison to mono-amphiphiles. Because of the unique molecular architecture, bolaamphiphiles should be more difficult to insert into the cell membrane, causing less membrane disruption. In contrast, mono-amphiphiles can insert into membrane more easily and cause membrane disruption due to their structural similarity to native phospholipids. (b) Hemolytic activity of both mono- and bolaamphiphiles as % hemolysis of bovine red blood cells. (c) Cytotoxicity of both mono- and bolaamphiphiles to NIH 3T3 cells as determined by MTT assay.

peptide headgroups to the central hydrophobic core to provide stimuli-responsive intracellular disassembly of the complexes, facilitating siRNA release in cytosol.<sup>47</sup>

## RESULTS AND DISCUSSION

A representative peptide bola structure (**bola-C18-G2**) is shown in Figure 1c. The amphiphiles are named as follows: m- for mono-amphiphile and bola- for bolaamphiphile, followed by the structure of the hydrophobic core (e.g., C18) and then the generation of the dendron headgroups (e.g., G2). Different hydrophobic cores were investigated, including hydrocarbon chains of various lengths (C6-C22) and a fluorocarbon core (**F10**). The length of the hydrophobic cores was chosen to be significantly shorter than the width of a typical phospholipid bilayer membrane so that bolas will not be able to span across the entire bilayer and cause cell membrane disruption. A control molecule containing a hexa(ethylene glycol) core (**HEG**) was included as the hydrophilic core should not induce self-assembly in aqueous solution. A hydrophobic core containing a 1,2,3-triazole (**TZ**) was also synthesized to probe the effect of the kinked backbone. The size of the dendron headgroup was varied from first to third generation (G1-G3). For a direct comparison between mono- and

bolaamphiphiles, three mono-amphiphile analogues were synthesized containing either a C11 alkyl tail (**m-C11**) or one to two oleic acid moieties (**m-OA** or **m-OA2**), with the structures shown in Figure 1d. It should be noted that linear peptide mono-amphiphiles have been extensively studied for self-assembly and biomaterials applications.<sup>48,49</sup> All molecules were synthesized by solution-phase coupling reactions, and detailed synthesis and characterization data can be found in the Supporting Information.

Our hypothesis of low membrane disruption for bolas was first tested by hemolysis assays. Bovine red blood cells (RBC) were treated with the amphiphiles at various concentrations, and the release of hemoglobin from the RBC was measured as an indicator of membrane lytic activity. Supporting our hypothesis, the mono-amphiphiles exhibited greater hemolytic activity than the bolas (Figure 2b). The hydrophobic tail of mono-amphiphiles significantly influenced their hemolytic activity, as the longer OA amphiphile exhibited 4 times higher membrane lysis than the shorter C11 amphiphile. The double tailed OA2 amphiphile induced a relatively high degree of hemolysis at lower concentrations, but plateaued at higher concentration, possibly due to self-assembly at higher concentration. In sharp contrast, the C18 bolas exhibited very

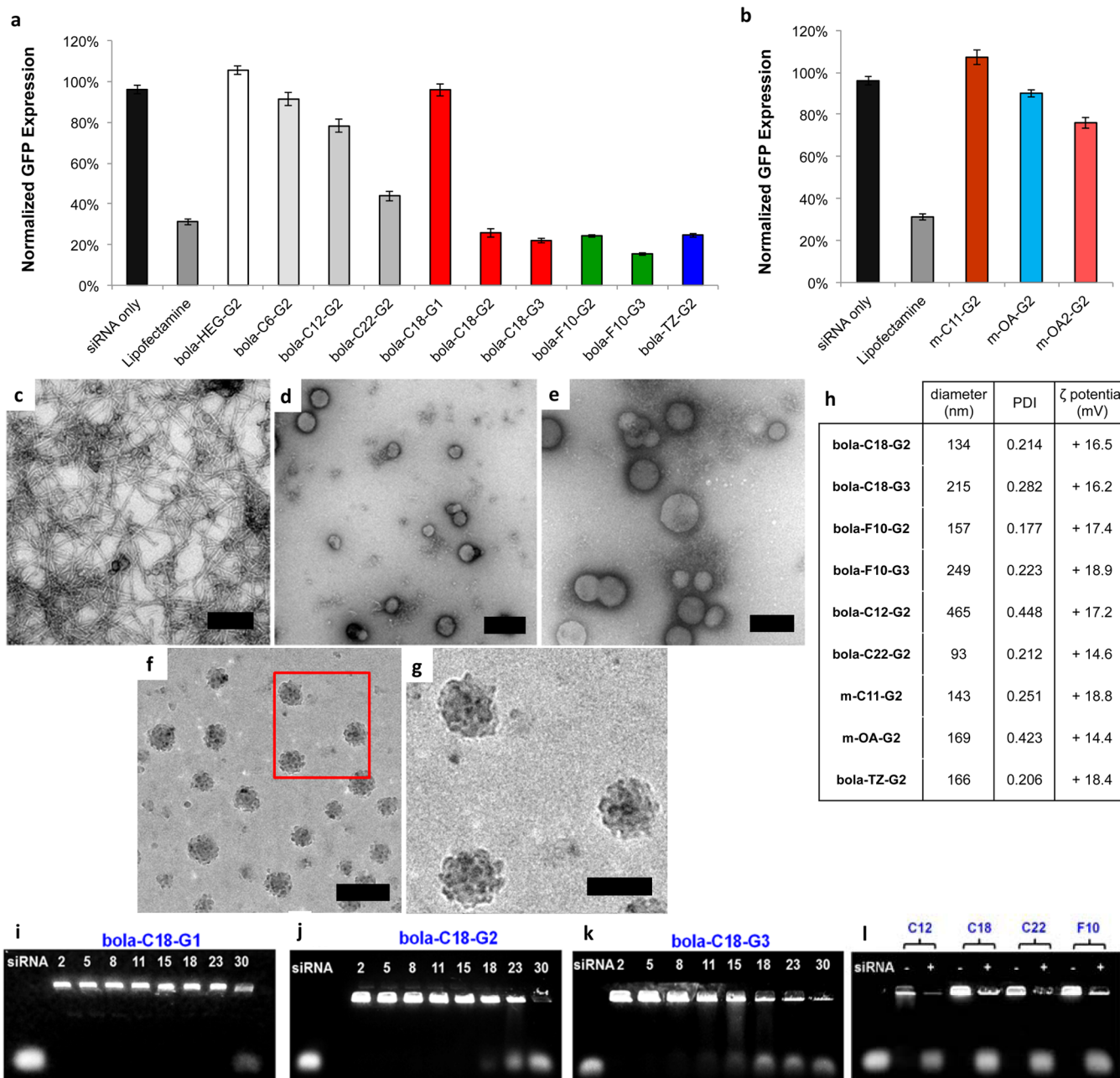


**Figure 3.** Transfection, TEM imaging, DLS analysis, and gel electrophoresis of different amphiphile/siRNA complexes. (a, b) Initial transfection screening of bola- and mono-amphiphiles in GFP-expressing NIH 3T3 cells. N/P ratio = 45 and [siRNA] = 100 nM. (c–e) Negative-stain TEM (uranyl acetate) images of vector/siRNA complexes: bola-C18-G1 (c), bola-C18-G2 (d), and bola-C18-G3 (e), scale bars = 200 nm. (f, g) Cryo-TEM imaging of bola-C18-G2 in PBS, scale bar = 200 nm (f) and 100 nm (g). (h) Dynamic light scattering (DLS) particle size and zeta potential analysis of vector/siRNA complexes prepared at N/P = 45 in PBS. (i–k) Dextran sulfate competitive binding assay with different bola complexes (N/P = 45) with the numbers above the wells indicating the S/P ratio (molar ratio of sulfate on dextran sulfate to phosphates on siRNA). (l) Triggered siRNA release by reducing reagent glutathione (GSH). Different bola-G2 complexes (N/P = 45, named by the core) were treated with GSH (+) or PBS (−) for 60 min before gel electrophoresis.

low hemolytic activity, with G2 inducing less than 1% hemolysis and G1 ≈ 3% hemolysis at 250  $\mu$ g/mL. The higher hemolysis induced by G1 bola agrees with our proposed headgroup size effect, as the small G1 dendron provides less steric hindrance to the U-shaped conformation. The different hemolytic activity of these dendron amphiphiles correlates well with their cytotoxicity. As shown in Figure 2c, all G2 bolaamphiphiles are about 2 orders of magnitude less cytotoxic to 3T3 fibroblast cells than the analogous mono-amphiphiles. The increased cytotoxicity of bola-C18-G3 is presumably due

to the higher valency of cationic charges of the G3 dendron. For comparison, branched PEI ( $M_n \approx 25$  kDa), a commonly used polymer for gene delivery studies, induces much greater toxicity than both mono- and bolaamphiphiles, further confirming the safety of bolas for siRNA delivery.

The mono- and bolaamphiphiles were screened for gene silencing activity in NIH 3T3 cells expressing green fluorescent protein (GFP). Initial transfection and gel electrophoresis experiments suggested that while most vectors fully complexed siRNA by N/P = 10 (the molar ratio of the charged amines of

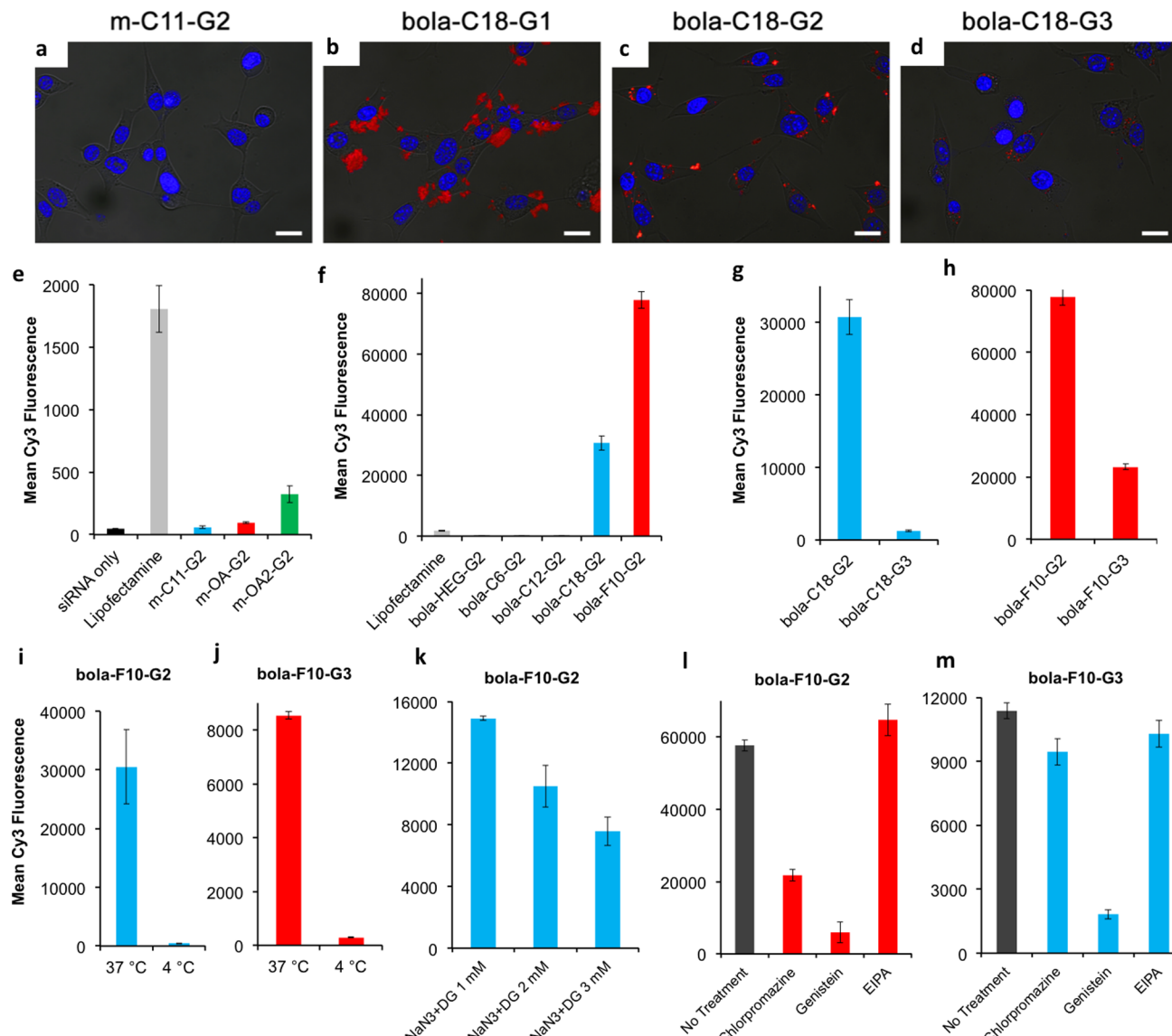


**Figure 4.** Cell uptake of different amphiphile/siRNA complexes. Cys3-siRNA was complexed with different amphiphiles and transfected to NIH 3T3 cells. (a–d) Confocal fluorescence images of transfected cells (cell nuclei were counter-stained with DAPI, scale bar: 20  $\mu$ m). (e, f) Cell uptake of siRNA complexes with different mono- and bolaamphiphiles quantified by flow cytometry. (g, h) Cell uptake of G2 and G3 bolaamphiphile vectors. (i, j) Transfection of Cy3-siRNA complexes carried out at 37 or 4 °C. (k) Transfection of 3T3 cells pretreated with sodium azide ( $\text{NaN}_3$ ) and 2-deoxy-D-glucose (DG). (l, m) Endocytic pathway of bola complexes. 3T3 cells were treated with chlorpromazine (30  $\mu$ M, inhibitor of clathrin-mediated endocytosis), genistein (350  $\mu$ M, inhibitor of caveolar endocytosis), or ethylisopropylamiloride (EIPA, 30  $\mu$ M, inhibitor of macropinocytosis) for 1 h before transfection of Cy3-siRNA/bola complexes.

the vector to the phosphates of RNA) the knockdown effect was not saturated until N/P = 30–45, and for all further studies a N/P ratio of 45 was utilized (Figure S1). For comparison to the toxicity and hemolysis assays, **bola-F10-G2** complexes formed at N/P = 45 with [siRNA] = 100 nM have a vector concentration of 110  $\mu$ g/mL, at which no significant toxic effect was observed (Figure 2c). In general, mono-amphiphiles showed very little gene silencing with the most efficacious, **m-OA2-G2**, inducing only ~25% knockdown (Figure 3b). In contrast, bolaamphiphiles containing the fluorocarbon (F10) or hydrocarbon cores of sufficient length (C18, C22) with G2 or G3 headgroups displayed effective gene silencing. The introduction of triazole ring in the hydrophobic core (TZ) did not significantly change the transfection efficiency. Bolaamphiphiles based on shorter cores (**bola-C6-G2** and **bola-C12-G2**) or bearing G1 headgroups failed to induce a

strong knockdown response (Figure 3a). The vector containing a hydrophilic linker (**bola-HEG-G2**) was completely ineffective at gene silencing, presumably due to the lack of hydrophobic self-assembly.

To understand the correlation between molecular structure and delivery efficiency, transmission electron microscopy (TEM) was utilized to examine the morphology of different amphiphile/siRNA complexes. Figure 3c–e displays TEM images of different **bola-C18**/siRNA complexes stained with uranyl acetate, demonstrating that the size of the dendritic headgroup influences the morphology of the assembled nanostructures dramatically. The compound with the smallest headgroup, **bola-C18-G1**, can pack closely to form twisted nanofibers, similar in morphology to the structures previously reported for well-packed bola assemblies (Figure 3c).<sup>35</sup> As the headgroup increases in size, both steric effects and charge

repulsion disfavor the formation of densely packed nanofibrils, with **bola-C18-G2** and **bola-C18-G3** complexes appearing as circular features consistent with assembly into nanoparticles (**Figure 3d,e**). The larger headgroup of G3 bolaamphiphiles further reduces the packing efficiency for the hydrophobic core, resulting in larger particles than G2 bolaamphiphiles. Complexes formed using G2 bolaamphiphiles containing fluorocarbon (**F10**) or 1,2,3-triazole (**TZ**) cores also displayed nanoparticle morphology (**Figure S2a–c**), as did both monoamphiphiles containing a single hydrophobic tail (**m-C11-G2**, **m-OA-G2**, **Figure S2d,e**). The **m-OA2-G2** complexes formed fibrillar structures similar to those observed in the **bola-C18-G1** images, potentially due to increased hydrophobic interactions from the additional oleate tail enhancing the stability of assembly (**Figure S2f**). Cryo-TEM was further used to observe the *in situ* morphology of the vector/siRNA complexes in PBS with **bola-C18-G2** chosen for initial analysis. The cryo-TEM images of **bola-C18-G2** (**Figure 3f,g**) complexes were characterized by nanoparticles with an average diameter of  $88 \pm 19$  nm, which appear to be composed of smaller “granules” approximately 10–20 nm in diameter. Nanoparticles displaying similar “raspberry” morphology have been observed for siRNA complexes of the peptide vector CADY.<sup>50</sup>

The particle size and zeta potential of the complexes were analyzed using dynamic light scattering (DLS) (**Figure 3h**). Complexes formed from vectors lacking a hydrophobic core or sufficient length (**bola-HEG-G2**, **bola-C6-G2**) did not provide enough signals for analysis, consistent with a lack of assembly. The complexes that formed fibrillar assemblies as observed by TEM (**bola-C18-G1**, **m-OA2-G2**) produced scattering signal, but the data did not correlate when analyzed via standard methods, possibly due to the formation of irregular aggregates or fibrillar networks. For both **bola-C18** and **bola-F10** vectors the particle size of G2 was smaller than that of the G3, while the particle size decreased with increasing length of alkyl core from **bola-C12-G2**, **bola-C18-G2**, to **bola-C22-G2**. The trend is consistent with proposed assembly stability, with smaller headgroup and longer hydrophobic core condensing siRNA into smaller particles and larger headgroup and shorter core into larger particles. The zeta potential of the vector/siRNA complexes was also measured, with all samples displaying a positive surface charge between 15 and 20 mV. Mono amphiphile/siRNA complexes, **m-C11-G2** and **m-OA-G2**, showed similar particle characteristics in DLS, with a slightly larger size than the bola analogue (**bola-C22-G2**).

In our bola design, we hypothesized that the more stable nanoparticles formed by bolaamphiphiles should enhance the siRNA binding strength, which was assessed via a competitive binding assay using the anionic polymer dextran sulfate (DS,  $M_n \approx 25$  kDa). Although **m-C11-G2** and **bola-C22-G2** have exactly the same chemical composition, the bola complexes exhibited much higher stability with little siRNA release up to S/P = 23 (the molar ratio of sulfate from DS and phosphate from siRNA), while the mono-amphiphile complex started to release siRNA at S/P = 8 (**Figure S3a,b**). Furthermore, the proposed self-assembly model agrees with the stability of different bola complexes. As shown in **Figure 3i–k**, despite having headgroups with the lowest level of multivalency, **bola-C18-G1** exhibited the strongest siRNA binding with no siRNA release up to S/P of 30, presumably due to the stable fibrillar assembly. The vectors **bola-C18-G2** and **bola-C18-G3**, which demonstrated nanoparticle assembly by TEM, showed siRNA release at the lower S/P ratios of 23 and 15, respectively. The

fluorocarbon vector, **bola-F10-G2**, demonstrated stronger siRNA binding than the hydrocarbon analogue **bola-C18-G2** with no siRNA release until S/P = 30 (**Figure S3c**), again presumably due to the more robust self-assembly induced by the fluorocarbon core. The bolaamphiphiles containing either the shortest hydrocarbon (**bola-C6-G2**) or hydrophilic core (**bola-HEG-G2**) failed to effectively complex siRNA (**Figure S3e,g**). Stimuli-responsive siRNA release from bola complexes was demonstrated by incubation of the complexes with glutathione (GSH) followed by subsequent gel electrophoresis, which showed effective decomplexation for the GSH treated samples (**Figure 3l**).

The different self-assembly behavior was corroborated by infrared (IR) spectroscopy. The methylene ( $\text{CH}_2$ ) groups in the alkyl region prefer *trans* conformation in highly ordered packing structure, resulting in lower frequency for their C–H stretching peaks.<sup>51</sup> **Figure S4** shows that from G1 to G3 bola complexes, both the asymmetric ( $\sim 2930 \text{ cm}^{-1}$ ) and symmetric ( $\sim 2850 \text{ cm}^{-1}$ ) C–H stretch peaks shifted to higher frequency, indicating less ordered structure in the alkyl region. This agrees with the proposed self-assembly model, with decreasing packing order from nanofibril to nanoparticle, caused by the enhanced electrostatic repulsion and sterics associated with increasing valency of the cationic dendron.

The cellular uptake of amphiphile-siRNA complexes was investigated by confocal fluorescence microscopy using Cy3 labeled siRNA (**Figure 4a–d**). The mono-amphiphile (**m-C11-G2**) complexes showed no cellular uptake with no detectable signal from Cy3-siRNA (**Figure 4a**), while **bola-C18-G1**/siRNA complexes formed aggregates on the cell surface and were not internalized (**Figure 4b**), in agreement with the observed low gene knockdown for both of these vectors (**Figure 3a,b**). Complexes formed with both **bola-C18-G2** and **bola-C18-G3** showed significant cellular uptake of siRNA, with G2 exhibiting higher efficiency (**Figure 4c,d**). The Cy3-siRNA uptake was further quantified by flow cytometry (**Figure 4e–h**). Compared to lipofectamine, Cy3-siRNA complexes with all three mono-amphiphiles showed very low cellular uptake (**Figure 4e**), while **bola-C18-G2** and **bola-F10-G2** exhibited 20–40 times higher uptake than lipofectamine (**Figure 4f**). Bolas with either shorter alkane cores (**C6** and **C12**) or a hydrophilic HEG core could not form stable complexes, and no cellular uptake of Cy3-siRNA was detected (**Figure 4f**). Notably, cell uptake efficiency was directly related to the size of headgroup. Both **boa-C18-G2** and **bola-F10-G2** showed much higher cell uptake than their G3 analogues (**Figure 4g,h**), which could be attributed to the higher stability and smaller size of G2 complexes.

To further understand the cell uptake process, we chose **bola-F10-G2** and **bola-F10-G3** as representative vectors to study the cell uptake pathway. **Figure 4i–k** shows that the cell uptake of bola/Cy3-siRNA complexes are energy dependent, with low temperature ( $4^\circ\text{C}$ ) completely shutting down the uptake (**Figure 4i,j**) and the metabolic inhibitor  $\text{NaN}_3$ /2-deoxy-D-glucose inhibiting uptake in a concentration-dependent manner (**Figure 4k**). The cell uptake mechanism was further studied by using several small molecule inhibitors to specifically block three common endocytotic pathways: clathrin-mediated endocytosis (chlorpromazine), caveolar endocytosis (genistein), and macropinocytosis (EIPA).<sup>52,53</sup> As shown in **Figure 4l,m**, siRNA/**bola-F10-G2** complexes were internalized through both clathrin-mediated and caveolar pathways. The **bola-F10-G3** complexes entered the cell through caveolae-

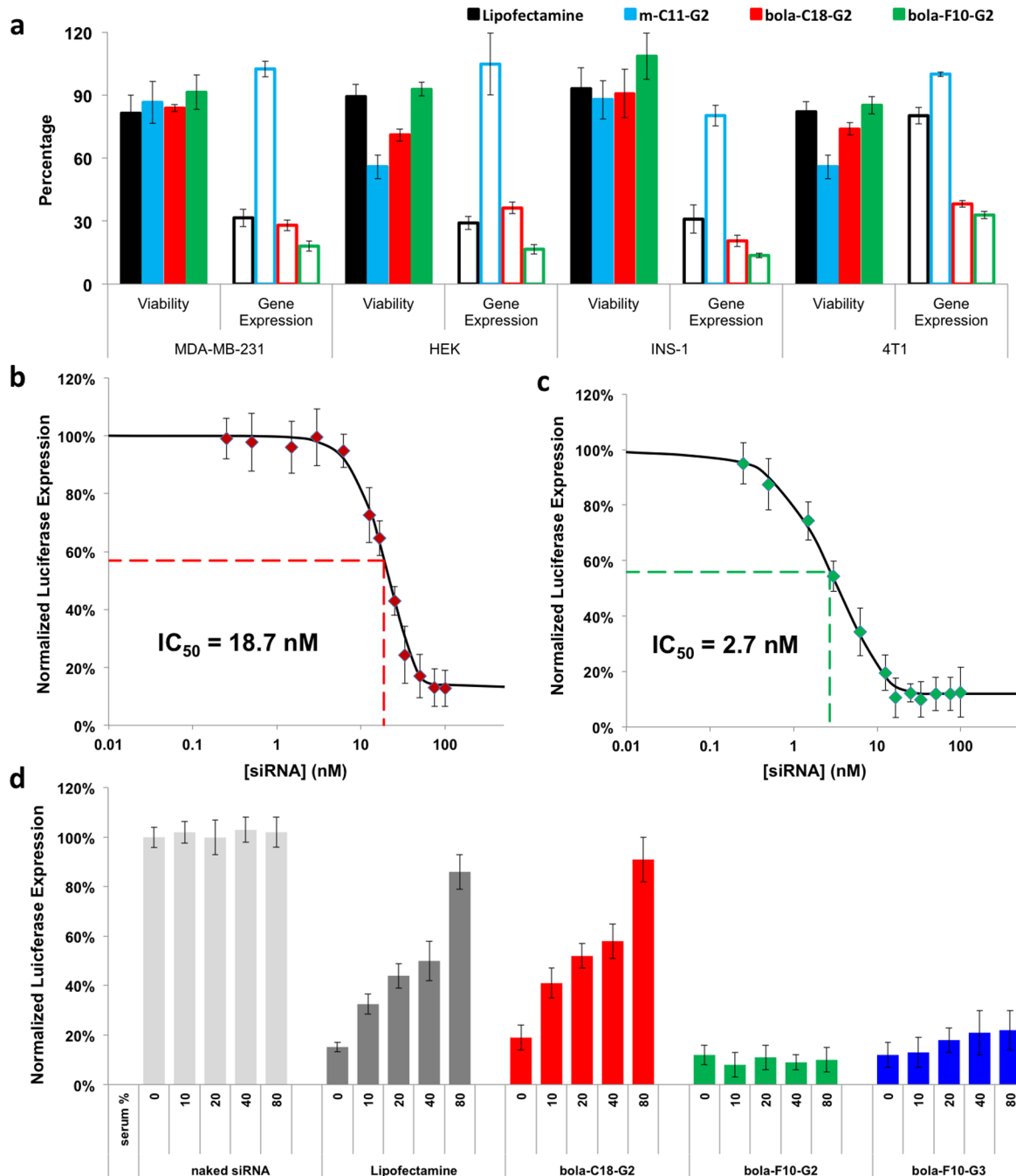


**Figure 5.** Transfection study in different cell lines and in the presence of serum. (a) Luciferase silencing data for various amphiphiles in different cell lines including MDA-MB-231, HEK 293,  $\beta$ -INS-1, and 4T1. N/P = 45, [siRNA] = 100 nM, viability measured by MTT assay. (b, c) Dose/response curves of bola-C18-G2 (b) and bola-F10-G2 (c) vectors in MDA-MB-231 cells. N/P = 45 for all samples, [siRNA] indicated on x-axis. (d) Transfection of MDA-MB-231 cells in serum-containing medium. N/P = 45, [siRNA] = 50 nM, final concentration of fetal bovine serum (FBS) in antibiotic-free DMEM transfection media indicated on the x-axis.

mediated endocytosis almost exclusively, which can be explained by the larger particle size of the bola-F10-G3 complexes.<sup>54,55</sup> The clear dependence of cell uptake on inhibitor concentration (Figure S5) further confirms the cellular uptake pathway.

To demonstrate the general efficacy of these vectors, transfections were carried out in the following luciferase-expressing cell lines: MDA-MB-231, HEK, INS-1, and 4T1 (Figure 5a). Similar to the results obtained from 3T3 cells, mono-amphiphile m-C11-G2 did not achieve any significant gene knockdown and induced substantial toxicity in HEK and

4T1 cells. In contrast, bolaamphiphiles C18-G2 and F10-G2 both displayed robust luciferase knockdown with minimal cytotoxicity. Notably, for the 4T1 cell line in which lipofectamine failed to induce a strong knockdown response, both C18-G2 and F10-G2 effectively silenced luciferase expression.

The previously discussed transfection studies used phosphate buffer (PBS, 10 mM phosphate, 10 mM NaCl, pH = 7.4) for sample preparation (Figure 3a,b and Figure 5a); however, it was observed during optimization that complexes prepared in OptiMEM induced significantly higher knockdown at low concentrations than those prepared in PBS. This optimized

**Table 1.** Structure–Property Relationship of Dendritic Peptide Amphiphiles for siRNA Delivery

molecular structure	assembly with siRNA	cell uptake	siRNA transfection	serum stability
mono-amphiphiles	nano particle/nanofibril	low cell uptake, highly membrane disruptive	low	
bolaamphiphile, small headgroup (G1)	nanofibril	aggregate on cell surface, no uptake	none	
bolaamphiphile, medium headgroup (G2)	smaller nanoparticle	clathrin- and caveolae-mediated endocytosis, high cell uptake	high efficiency	high
bolaamphiphile, large headgroup (G3)	larger nanoparticle	caveolae-mediated endocytosis, low cell uptake	high efficiency	low

protocol was used to further test the transfection efficiency of the vectors in MDA-MB-231 cells, with dose/response curves and IC<sub>50</sub> values determined for **bola-C18-G2**, **bola-C18-G3**, **bola-F10-G2**, and **bola-F10-G3**. The fluorocarbon vector **bola-F10-G2** demonstrated highly efficient transfection with an IC<sub>50</sub> value of 2.7 nM, while the analogous hydrocarbon vector, **bola-C18-G2**, was less effective with an IC<sub>50</sub> of 18.7 nM (Figure S<sub>b,c</sub>). For both C18 and F10 cores, the G3 variants displayed higher transfection efficiency than the corresponding G2 analogues, with calculated IC<sub>50</sub> values of 1.0 nM and 7.4 nM for **bola-F10-G3** and **bola-C18-G2**, respectively (Figure S<sub>6</sub>). These results suggest that the fluorocarbon linker greatly enhanced the delivery efficiency, with both F10 vectors displaying IC<sub>50</sub> values ~7 times lower than the corresponding hydrocarbon analogues. The toxicity of the bolaamphiphile/siRNA complexes prepared using OptiMEM was assessed via the MTT assay, with the results corroborating the previously observed trend of G3 inducing greater cytotoxicity than G2 for both C18 and F10 linkers (Figure S<sub>7</sub>).

Although typical *in vitro* transections are performed in reduced serum or serum-free media, successful transfection in the presence of negatively charged serum components is critical for *in vivo* application. To investigate the serum stability of our vectors, transfections were performed varying the final concentration of fetal bovine serum (FBS) in the transfection media from 0 to 80% (Figure S<sub>d</sub>). While lipofectamine RNAiMAX and **bola-C18-G2** were negatively affected even at low serum content, the gene silencing effects of **bola-F10-G2** were not affected by the presence of up to 80% FBS. The analogous G3 variant, **bola-F10-G3**, showed a slight decrease in efficacy at higher FBS concentrations, which can be attributed to less stable assembly and consequentially weaker siRNA binding due to the larger dendritic headgroup. The improved serum stability and efficacy of our fluorocarbon bolaamphiphiles compared to those containing hydrocarbon cores are in agreement with previous reports on the use of fluorinated lipids for siRNA delivery.<sup>44</sup> With recent reports of fluorination greatly enhancing DNA transfection efficiency of PAMAM dendrimers,<sup>45,46</sup> we believe this “fluorocarbon effect” may be generally applicable to other amphiphilic vectors.

On the basis of the data presented in this paper, a structure–property relationship can be derived for dendritic peptide amphiphiles for siRNA delivery (Table 1). Compared to the mono-amphiphiles studied, all G2 bolaamphiphiles of similar length displayed stronger siRNA binding, reduced cytotoxicity, and greatly enhanced transfection efficiency. The size of the cationic dendron was observed to have a major influence on the morphology and biological activity of the complexes, with the fibrillar assemblies formed by **bola-C18-G1** affording dramatically less knockdown than the nanoparticle **bola-C18-G2** and **bola-C18-G3** complexes (Table 1). While both G2 and G3 bolaamphiphiles are highly efficient for siRNA transfection, G2 vectors exhibit much higher serum stability than G3 analogues. The use of a fluorocarbon, as opposed to hydrocarbon core

greatly enhanced both the transfection efficacy and serum stability of the complexes, suggesting that further investigation into fluorocarbon-based vectors may prove particularly fruitful.

## CONCLUSION

With the high siRNA transfection efficiency in multiple cell lines, excellent serum resistance, and low cytotoxicity and hemolysis, the dendritic peptide bolaamphiphiles presented in this study are promising candidates for further gene delivery applications. Through a rational design approach, we were able to directly link the molecular structure of different vectors to their assembly morphologies and the resulting biological activities (Table 1). The unique bolaamphiphile architecture proved a key factor for improved complex stability, low cytotoxicity and hemolytic activity, and high transfection efficiency. The optimal vector contains a fluorocarbon core and exhibited enhanced delivery efficiency to a variety of cell lines and improved serum resistance when compared to hydrocarbon analogues and lipofectamine RNAiMAX. The high transfection efficiency of the fluorocarbon vectors and the direct correlation from molecular structure to self-assembly behavior to subsequent biologic activity offer critical insight aiding the rational design of new materials for nucleic acid delivery and other biomaterial applications.

## METHODS

**Amphiphile/siRNA Complex Preparation (PBS).** The 5× complex solution for transfection was prepared by pipet mixing of the amphiphile and siRNA solutions. In a typical procedure, 1.5 μM siRNA solution was prepared with PBS buffer (10 mM phosphate, 10 mM NaCl, pH = 7.4). Different amphiphile solutions (5 mg/mL) were diluted with PBS buffer to a final volume of 13.3 μL per well. The 13.3 μL of amphiphile solution was then added to 6.7 μL of 1.5 μM siRNA solution (final 5× siRNA concentration = 500 nM), followed by brief vortexing. The solution was incubated at room temperature for 30 min before addition to the cell culture media.

**Optimized Complex Preparation (OptiMEM).** The vector/siRNA complexes were prepared by first diluting the vector to the desired concentration using antibiotic-free OptiMEM. The siRNA was diluted to 1.5 μM with OptiMEM, and an appropriate amount of this solution was added to the diluted vector to give a complex solution with siRNA concentration of 500 nM. After 10 min incubation, this complex solution was further diluted to the desired concentration with OptiMEM and used immediately.

**Transfection and Flow Cytometry.** NIH 3T3 fibroblast cells were seeded at a density of 10 000 cells/well in 48-well plates 24 h in advance. Prior to transfection, the media was replaced with 80 μL of antibiotic-free DMEM, and 20 μL of the previously described 5× complex solutions were added to each well to give 100 nM final siRNA concentration. After 4 h

incubation, the medium was changed back to 250  $\mu\text{L}$  of DMEM supplemented with 10% fetal bovine serum and cultured for another 48 h. Before the analysis, cells were released from each well by Trypsin and harvested by centrifugation (5 min, 500g). Fluorescence of transfected cells was measured on a Becton-Dickinson LSR II flow cytometer with argon ion excitation laser. For each sample, data representing 10 000 objects were collected as a list-mode file and analyzed using FACSDivaTM software. The normalized GFP expression was calculated by comparing cells treated with anti-GFP siRNA complexes to a control sample treated with complexes prepared with nontargeting siRNA.

## ■ ASSOCIATED CONTENT

### Supporting Information

The Supporting Information is available free of charge on the ACS Publications website at DOI: [10.1021/acscentsci.5b00233](https://doi.org/10.1021/acscentsci.5b00233).

Experimental details, synthesis and characterization data, gel and TEM images, transfection data, and IR and NMR spectra ([PDF](#))

## ■ AUTHOR INFORMATION

### Corresponding Author

\*E-mail: [zguan@uci.edu](mailto:zguan@uci.edu).

### Author Contributions

<sup>†</sup>H.Z. and M.E.J. contributed equally to this work.

### Notes

The authors declare no competing financial interest.

## ■ ACKNOWLEDGMENTS

We acknowledge the financial support of the U.S. National Institute of Health (DK098446). We thank Professor Young Jik Kwon for donating the GFP-expressing NIH 3T3 cell, Professor Jennifer Prescher for donating the luciferase-expressing HEK, MDA-MB-231, 4T1, and Professor Yoko Mullen for donating INS-1 cells.

## ■ REFERENCES

- (1) Sahin, Ö.; Löbke, C.; Korf, U.; Appelhans, H.; Sültmann, H.; Poustka, A.; Wiemann, S.; Arlt, D. Combinatorial RNAi for quantitative protein network analysis. *Proc. Natl. Acad. Sci. U. S. A.* **2007**, *104*, 6579–6584.
- (2) Dietzl, G.; Chen, D.; Schnorrer, F.; Su, K.-C.; Barinova, Y.; Fellner, M.; Gasser, B.; Kinsey, K.; Oppel, S.; Scheiblauer, S.; Couto, A.; Marra, V.; Keleman, K.; Dickson, B. J. A genome-wide transgenic RNAi library for conditional gene inactivation in *Drosophila*. *Nature* **2007**, *448*, 151–156.
- (3) Chen, T.; Heller, E.; Beronja, S.; Oshimori, N.; Stokes, N.; Fuchs, E. An RNA interference screen uncovers a new molecule in stem cell self-renewal and long-term regeneration. *Nature* **2012**, *485*, 104–108.
- (4) Castanotto, D.; Rossi, J. J. The promises and pitfalls of RNA-interference-based therapeutics. *Nature* **2009**, *457*, 426–433.
- (5) de Fougerolles, A.; Vornlocher, H.-P.; Maraganore, J.; Lieberman, J. Interfering with disease: a progress report on siRNA-based therapeutics. *Nat. Rev. Drug Discovery* **2007**, *6*, 443–453.
- (6) Whitehead, K. A.; Langer, R.; Anderson, D. G. Knocking down barriers: advances in siRNA delivery. *Nat. Rev. Drug Discovery* **2009**, *8*, 129–138.
- (7) Mitragotri, S.; Burke, P. A.; Langer, R. Overcoming the challenges in administering biopharmaceuticals: formulation and delivery strategies. *Nat. Rev. Drug Discovery* **2014**, *13*, 655–672.
- (8) Kanasty, R.; Dorkin, J. R.; Vegas, A.; Anderson, D. Delivery materials for siRNA therapeutics. *Nat. Mater.* **2013**, *12*, 967–977.
- (9) Malone, R. W.; Felgner, P. L.; Verma, I. M. Cationic liposome-mediated RNA transfection. *Proc. Natl. Acad. Sci. U. S. A.* **1989**, *86*, 6077–6081.
- (10) Love, K. T.; Mahon, K. P.; Levins, C. G.; Whitehead, K. A.; Querbes, W.; Dorkin, J. R.; Qin, J.; Cantley, W.; Qin, L. L.; Racie, T.; Frank-Kamenetsky, M.; Yip, K. N.; Alvarez, R.; Sah, D. W. Y.; de Fougerolles, A.; Fitzgerald, K.; Kotliansky, V.; Akinc, A.; Langer, R.; Anderson, D. G. Lipid-like materials for low-dose, *in vivo* gene silencing. *Proc. Natl. Acad. Sci. U. S. A.* **2010**, *107*, 1864–1869.
- (11) Semple, S. C.; Akinc, A.; Chen, J.; Sandhu, A. P.; Mui, B. L.; Cho, C. K.; Sah, D. W. Y.; Stebbing, D.; Crosley, E. J.; Yaworski, E.; Hafez, I. M.; Dorkin, J. R.; Qin, J.; Lam, K.; Rajeev, K. G.; Wong, K. F.; Jeffs, L. B.; Nechev, L.; Eisenhardt, M. L.; Jayaraman, M.; Kazem, M.; Maier, M. A.; Srinivasulu, M.; Weinstein, M. J.; Chen, Q.; Alvarez, R.; Barros, S. A.; De, S.; Klimuk, S. K.; Borland, T.; Kosovrasti, V.; Cantley, W. L.; Tam, Y. K.; Manoharan, M.; Ciufolini, M. A.; Tracy, M. A.; de Fougerolles, A.; MacLachlan, I.; Cullis, P. R.; Madden, T. D.; Hope, M. J. Rational design of cationic lipids for siRNA delivery. *Nat. Biotechnol.* **2010**, *28*, 172–176.
- (12) Crombez, L.; Aldrian-Herrada, G.; Konate, K.; Nguyen, Q. N.; McMaster, G. K.; Brasseur, R.; Heitz, F.; Divita, G. A New Potent Secondary Amphiphatic Cell-penetrating Peptide for siRNA Delivery Into Mammalian Cells. *Mol. Ther.* **2009**, *17*, 95–103.
- (13) Eguchi, A.; Dowdy, S. F. siRNA delivery using peptide transduction domains. *Trends Pharmacol. Sci.* **2009**, *30*, 341–345.
- (14) Won, Y.-W.; Adhikary, P. P.; Lim, K. S.; Kim, H. J.; Kim, J. K.; Kim, Y.-H. Oligopeptide complex for targeted non-viral gene delivery to adipocytes. *Nat. Mater.* **2014**, *13*, 1157–1164.
- (15) Kumar, P.; Wu, H.; McBride, J. L.; Jung, K.-E.; Hee Kim, M.; Davidson, B. L.; Kyung Lee, S.; Shankar, P.; Manjunath, N. Transvascular delivery of small interfering RNA to the central nervous system. *Nature* **2007**, *448*, 39–43.
- (16) Davis, M. E.; Zuckerman, J. E.; Choi, C. H. J.; Seligson, D.; Tolcher, A.; Alabi, C. A.; Yen, Y.; Heidel, J. D.; Ribas, A. Evidence of RNAi in humans from systemically administered siRNA via targeted nanoparticles. *Nature* **2010**, *464*, 1067–1070.
- (17) Rozema, D. B.; Lewis, D. L.; Wakefield, D. H.; Wong, S. C.; Klein, J. J.; Roesch, P. L.; Bertin, S. L.; Reppen, T. W.; Chu, Q.; Blokhin, A. V.; Hagstrom, J. E.; Wolff, J. A. Dynamic PolyConjugates for targeted *in vivo* delivery of siRNA to hepatocytes. *Proc. Natl. Acad. Sci. U. S. A.* **2007**, *104*, 12982–12987.
- (18) Tschiche, A.; Malhotra, S.; Haag, R. Nonviral gene delivery with dendritic self-assembling architectures. *Nanomedicine* **2014**, *9*, 667–693.
- (19) Kulkarni, A.; DeFrees, K.; Hyun, S.-H.; Thompson, D. H. Pendant Polymer:Amino- $\beta$ -Cyclodextrin:siRNA Guest:Host Nanoparticles as Efficient Vectors for Gene Silencing. *J. Am. Chem. Soc.* **2012**, *134*, 7596–7599.
- (20) Wu, J.; Huang, W.; He, Z. Dendrimers as carriers for siRNA delivery and gene silencing: a review. *Sci. World J. [Online]* **2013**, *630654*. [10.1155/2013/630654](https://doi.org/10.1155/2013/630654)
- (21) Yu, T.; Liu, X.; Bolcato-Bellemin, A.-L.; Wang, Y.; Liu, C.; Erbacher, P.; Qu, F.; Rocchi, P.; Behr, J.-P.; Peng, L. An Amphiphilic Dendrimer for Effective Delivery of Small Interfering RNA and Gene Silencing In Vitro and In Vivo. *Angew. Chem., Int. Ed.* **2012**, *51*, 8478–8484.
- (22) Giljohann, D. A.; Seferos, D. S.; Prigodich, A. E.; Patel, P. C.; Mirkin, C. A. Gene Regulation with Polyvalent siRNA–Nanoparticle Conjugates. *J. Am. Chem. Soc.* **2009**, *131*, 2072–2073.
- (23) Kim, S. T.; Chompoosor, A.; Yeh, Y.-C.; Agasti, S. S.; Solfield, D. J.; Rotello, V. M. Dendronized Gold Nanoparticles for siRNA Delivery. *Small* **2012**, *8*, 3253–3256.
- (24) Dokka, S.; Toledo, D.; Shi, X.; Castranova, V.; Rojanasakul, Y. Oxygen Radical-Mediated Pulmonary Toxicity Induced by Some Cationic Liposomes. *Pharm. Res.* **2000**, *17*, 521–525.
- (25) Landesman-Milo, D.; Peer, D. Toxicity profiling of several common RNAi-based nanomedicines: a comparative study. *Drug Delivery Transl. Res.* **2014**, *4*, 96–103.

- (26) Lv, H. T.; Zhang, S. B.; Wang, B.; Cui, S. H.; Yan, J. Toxicity of cationic lipids and cationic polymers in gene delivery. *J. Controlled Release* **2006**, *114*, 100–109.
- (27) Tabernero, J.; Shapiro, G. I.; LoRusso, P. M.; Cervantes, A.; Schwartz, G. K.; Weiss, G. J.; Paz-Ares, L.; Cho, D. C.; Infante, J. R.; Alsina, M.; Gounder, M. M.; Falzone, R.; Harrop, J.; White, A. C. S.; Toudjarska, I.; Bumcrot, D.; Meyers, R. E.; Hinkle, G.; Svrzikapa, N.; Hutabarat, R. M.; Clausen, V. A.; Cehelsky, J.; Nochur, S. V.; Gambavitalo, C.; Vaishnav, A. K.; Sah, D. W. Y.; Gollob, J. A.; Burris, H. A. First-in-Humans Trial of an RNA Interference Therapeutic Targeting VEGF and KSP in Cancer Patients with Liver Involvement. *Cancer Discovery* **2013**, *3*, 406–417.
- (28) Wong, S. C.; Klein, J. J.; Hamilton, H. L.; Chu, Q.; Frey, C. L.; Trubetskoy, V. S.; Hegge, J.; Wakefield, D.; Rozema, D. B.; Lewis, D. L. Co-injection of a targeted, reversibly masked endosomolytic polymer dramatically improves the efficacy of cholesterol-conjugated small interfering RNAs *in vivo*. *Nucleic Acid Ther.* **2012**, *22*, 380–390.
- (29) Gilleron, J.; Querbes, W.; Zeigerer, A.; Borodovsky, A.; Marsico, G.; Schubert, U.; Manygoats, K.; Seifert, S.; Andree, C.; Stoter, M.; Epstein-Barash, H.; Zhang, L.; Koteliansky, V.; Fitzgerald, K.; Fava, E.; Bickle, M.; Kalaidzidis, Y.; Akinc, A.; Maier, M.; Zerial, M. Image-based analysis of lipid nanoparticle-mediated siRNA delivery, intracellular trafficking and endosomal escape. *Nat. Biotechnol.* **2013**, *31*, 638–646.
- (30) Shete, H. K.; Prabhu, R. H.; Patravale, V. B. Endosomal Escape: A Bottleneck in Intracellular Delivery. *J. Nanosci. Nanotechnol.* **2014**, *14*, 460–474.
- (31) Hafez, I. M.; Maurer, N.; Cullis, P. R. On the mechanism whereby cationic lipids promote intracellular delivery of polynucleic acids. *Gene Ther.* **2001**, *8*, 1188–1196.
- (32) Knudsen, K. B.; Northeved, H.; Kumar EK, P.; Permin, A.; Gjetting, T.; Andresen, T. L.; Larsen, S.; Wegener, K. M.; Lykkesfeldt, J.; Jantzen, K.; Loft, S.; Moller, P.; Roursgaard, M. In vivo toxicity of cationic micelles and liposomes. *Nanomedicine* **2015**, *11*, 467–477.
- (33) Hunter, A. C. Molecular hurdles in polyfector design and mechanistic background to polycation induced cytotoxicity. *Adv. Drug Delivery Rev.* **2006**, *58*, 1523–1531.
- (34) Dong, Y. Z.; Love, K. T.; Dorkin, J. R.; Sirirungruang, S.; Zhang, Y. L.; Chen, D. L.; Bogorad, R. L.; Yin, H.; Chen, Y.; Vegas, A. J.; Alabi, C. A.; Sahay, G.; Olejnik, K. T.; Wang, W. H.; Schroeder, A.; Lytton-Jean, A. K. R.; Siegwart, D. J.; Akinc, A.; Barnes, C.; Barros, S. A.; Carioto, M.; Fitzgerald, K.; Hettinger, J.; Kumar, V.; Novobrantseva, T. I.; Qin, J. N.; Querbes, W.; Koteliansky, V.; Langer, R.; Anderson, D. G. Lipopeptide nanoparticles for potent and selective siRNA delivery in rodents and nonhuman primates. *Proc. Natl. Acad. Sci. U. S. A.* **2014**, *111*, 3955–3960.
- (35) Nuraje, N.; Bai, H. Y.; Su, K. Bolaamphiphilic molecules: Assembly and applications. *Prog. Polym. Sci.* **2013**, *38*, 302–343.
- (36) Valentine, D. L. Adaptations to energy stress dictate the ecology and evolution of the Archaea. *Nat. Rev. Microbiol.* **2007**, *5*, 316–323.
- (37) Jain, N.; Goldschmidt, V.; Oncul, S.; Arntz, Y.; Duportail, G.; Mely, Y.; Klymchenko, A. S. Lactose-ornithine bolaamphiphiles for efficient gene delivery *in vitro*. *Int. J. Pharm.* **2012**, *423*, 392–400.
- (38) Khan, M.; Ang, C. Y.; Wiradharma, N.; Yong, L. K.; Liu, S. Q.; Liu, L. H.; Gao, S. J.; Yang, Y. Y. Diaminododecane-based cationic bolaamphiphile as a non-viral gene delivery carrier. *Biomaterials* **2012**, *33*, 4673–4680.
- (39) Kim, T.; Afonin, K. A.; Viard, M.; Koyfman, A. Y.; Sparks, S.; Heldman, E.; Grinberg, S.; Linder, C.; Blumenthal, R. P.; Shapiro, B. A. In Silico, In Vitro, and In Vivo Studies Indicate the Potential Use of Bolaamphiphiles for Therapeutic siRNAs Delivery. *Mol. Ther.-Nucleic Acids* **2013**, *2*, e80. 10.1038/mtna.2013.5
- (40) Popov, M.; Abu Hammad, I.; Bachar, T.; Grinberg, S.; Linder, C.; Stepensky, D.; Heldman, E. Delivery of analgesic peptides to the brain by nano-sized bolaamphiphilic vesicles made of monolayer membranes. *Eur. J. Pharm. Biopharm.* **2013**, *85*, 381–389.
- (41) Zeng, H.; Little, H. C.; Tiambeng, T. N.; Williams, G. A.; Guan, Z. Multifunctional Dendronized Peptide Polymer Platform for Safe and Effective siRNA Delivery. *J. Am. Chem. Soc.* **2013**, *135*, 4962–4965.
- (42) Saito, H.; Shinoda, W.; Mikami, M. Enhanced Hydrophobicity of Fluorinated Lipid Bilayer: A Molecular Dynamics Study. *J. Phys. Chem. B* **2008**, *112*, 11305–11309.
- (43) Dafik, L.; Kalsani, V.; Leung, A. K. L.; Kumar, K. Fluorinated Lipid Constructs Permit Facile Passage of Molecular Cargo into Living Cells. *J. Am. Chem. Soc.* **2009**, *131*, 12091–12093.
- (44) Klein, E.; Leborgne, C.; Ciobanu, M.; Klein, J.; Frisch, B.; Pons, F.; Zuber, G.; Scherman, D.; Kichler, A.; Lebeau, L. Nucleic acid transfer with hemifluorinated polycationic lipids. *Biomaterials* **2010**, *31*, 4781–4788.
- (45) Wang, M.; Liu, H.; Li, L.; Cheng, Y. A fluorinated dendrimer achieves excellent gene transfection efficacy at extremely low nitrogen to phosphorus ratios. *Nat. Commun.* **2014**, *5*. 10.1038/ncomms4053
- (46) Saito, H.; Shinoda, W.; Mikami, M. Fluorination effects on structure and dynamics of phospholipid bilayer: A molecular dynamics study. *Chem. Phys. Lett.* **2009**, *468*, 260–263.
- (47) Son, S.; Namgung, R.; Kim, J.; Singha, K.; Kim, W. J. Bioreducible Polymers for Gene Silencing and Delivery. *Acc. Chem. Res.* **2012**, *45*, 1100–1112.
- (48) Hartgerink, J. D.; Beniash, E.; Stupp, S. I. Self-assembly and mineralization of peptide-amphiphile nanofibers. *Science* **2001**, *294*, 1684–1688.
- (49) Silva, G. A.; Czeisler, C.; Niece, K. L.; Beniash, E.; Harrington, D. A.; Kessler, J. A.; Stupp, S. I. Selective differentiation of neural progenitor cells by high-epitope density nanofibers. *Science* **2004**, *303*, 1352–1355.
- (50) Deshayes, S.; Konate, K.; Rydström, A.; Crombez, L.; Godefroy, C.; Milhiet, P.-E.; Thomas, A.; Brasseur, R.; Aldrian, G.; Heitz, F.; Muñoz-Morris, M. A.; Devoisselle, J.-M.; Divita, G. Self-Assembling Peptide-Based Nanoparticles for siRNA Delivery in Primary Cell Lines. *Small* **2012**, *8*, 2184–2188.
- (51) Liu, X. F.; Wang, T. Y.; Liu, M. H. Interfacial Assembly of a Series of Cinnamoyl-Containing Bolaamphiphiles: Spacer-Controlled Packing, Photochemistry, and Odd–Even Effect. *Langmuir* **2012**, *28*, 3474–3482.
- (52) Khalil, I. A.; Kogure, K.; Akita, H.; Harashima, H. Uptake pathways and subsequent intracellular trafficking in nonviral gene delivery. *Pharmacol. Rev.* **2006**, *58*, 32–45.
- (53) Ivanov, A. In *Exocytosis and Endocytosis*; Ivanov, A., Ed.; Humana Press: 2008; Vol. 440, p 15.
- (54) Rejman, J.; Oberle, V.; Zuhorn, I. S.; Hoekstra, D. Size-dependent internalization of particles via the pathways of clathrin- and caveolae-mediated endocytosis. *Biochem. J.* **2004**, *377*, 159–169.
- (55) Rehman, Z. u.; Zuhorn, I. S.; Hoekstra, D. How cationic lipids transfer nucleic acids into cells and across cellular membranes: Recent advances. *J. Controlled Release* **2013**, *166*, 46–56.
- (56) Wang, M.; Cheng, Y. The effect of fluorination on the transfection efficacy of surface-engineered dendrimers. *Biomaterials* **2014**, *35*, 6603–6613.